Quasifree $(p,2p)$ and (p,pn) reactions with unstable nuclei

T. Aumann,[1,2,*] C. A. Bertulani,[3,†] and J. Ryckebusch[4,‡]

[1]*Institut für Kernphysik, Technische Universität Darmstadt, Schlossgartenstr. 9, 64289 Darmstadt, Germany*

[2]*GSI Helmholtzzentrum für Schwerionenforschung, Planckstr. 1, 64291 Darmstadt, Germany*

[3]*Texas A&M University-Commerce, PO Box 3011, Commerce, Texas 75429, USA*

[4]*Department of Physics and Astronomy, Ghent University, B-9000 Gent, Belgium*

(Received 28 September 2013; published 17 December 2013)

We study $(p,2p)$ and (p,pn) reactions at proton energies in the range of 100 MeV–1 GeV. Our purpose is to explore the most sensitive observables in unpolarized reactions with inverse kinematics involving radioactive nuclei. We formulate a model based on the eikonal theory to describe total cross sections and momentum distributions of the recoiled residual nucleus. The model is similar to the one adopted for knockout reactions with heavy ions. We show that momentum distributions are sensitive to the angular momentum of the ejected nucleon which can be used as an spectroscopic tool. The total cross sections are sensitive to the nucleon separation energies and to multiple scattering effects. Our calculations also indicate that a beam energy around 500 MeV/nucleon has a smaller dependence on the anisotropy of the nucleon-nucleon elastic scattering.

DOI: 10.1103/PhysRevC.88.064610 PACS number(s): 25.40.Ep, 25.60.Dz, 25.60.Je, 24.10.−i

I. INTRODUCTION

Quasifree (p, pN) reactions (N = proton or neutron) represent one of the most common experimental tools to access information on single-particle properties in nuclei. In quasifree (p, pN) scattering an incident proton of medium energy (typically several hundred MeV) knocks out a bound nucleon. The energy spectrum of the outgoing nucleons provides information on the energy and other quantum numbers of the struck nucleon in the nucleus. The shape of the angular correlations of the outgoing nucleons, or the recoil momentum of the nucleus, is connected to the momentum distribution of the knocked-out nucleon. In the past four decades quasifree-scattering experiments have been performed with this basic purpose. For seminal reviews on (p,pn) reactions see, e.g., Refs. [1,2].

The theory developments in $(p,2p)$ reactions have been largely done in the past 50 years. Very few theorists still work in this field, basically due to the decrease in the number of experiments carried out in such a fashion. However, the availability of high-energy radioactive beams allows in principle to utilize the method of quasifree scattering in inverse kinematics with hydrogen targets. This will open huge possibilities to investigate properties of unstable nuclei such as systematic studies of single-particle structure or nucleon-nucleon correlations as a function of neutron-to-proton asymmetry.

So far, knockout reactions using composite targets have been used extensively to investigate the shell structure of rare isotopes and many valuable results have been obtained [3,4]. Gade *et al.* [4] have discussed, for instance, the reduction of spectroscopic strength in dependence on the asymmetry of the neutron and proton Fermi energies deduced from measured knockout cross sections. Theoretically, such an effect is indeed expected both for nuclei [5,6] and asymmetric nuclear matter [7]; the predicted effects, however, cannot explain the data.

Quasifree scattering in inverse kinematics potentially provides a more sensitive tool to study such effects since the reaction is less surface dominated. The possibility to detect all outgoing particles can provide a kinematically complete measurement of the reaction. At GSI, RIKEN, and other laboratories, experiments are being planned to study such effects more systematically and by applying a kinematically complete measurement of quasifree knockout reactions [8–10], and first pilot experiments were successful [10,11]. In order to extract the physics observables from the measured $(p,2p)$ and (p,pn) cross sections, reaction theory plays a key role. However, much of the theoretical expertise in this field was lost. It is thus imperative for the community to concentrate theoretical efforts in this problem with aim at the upcoming experiments with radioactive beams.

The framework of the distorted wave impulse approximation (DWIA) is often used in numerical calculations of (p, pN) reactions [12,13]. This method assumes that the dominant mechanism for the knockout reaction is due to a single interaction between the incident particle and the struck nucleon. The effect of the coherent multiple scattering with the other nucleons is incorporated by using distorted waves calculated from a mean nuclear potential, including absorption due to excitations to other channels. One also needs to account for the medium modification of interaction between the incoming proton and the struck nucleon [14–22].

A part of the difficulties in studying $(p,2p)$ and (p, pn) reactions relies on the uncertainty of in-medium interactions, and ambiguities from the reaction mechanism. Even in the energy region of several hundred MeV, where the NN cross section shows its minimum and the reaction mechanism is expected to be simplest, multistep processes are not negligible in general [23–27,35].

Measurements of polarization observables in quasielastic $(p,2p)$ reaction at intermediate energies give an even better

*t.aumann@gsi.de
†carlos.bertulani@tamuc.edu
‡jan.ryckebusch@ugent.be

information on nuclear shell structure and multiple scattering effects, and also on possible modification of the nucleon-nucleon (NN) interaction parameters in nuclear medium [23,35]. Due to the nuclear spin-orbit coupling and absorption of the projectile and secondary protons in the nuclear matter the proton knocked out from a particular nuclear shell with orbital moment $l \neq 0$ can be polarized [1,2,26–29].

In the next sections we describe a formalism for quasifree knockout reactions, first by describing the state-of-the-art DWIA method which has been shown to reproduce experimental data with a good accuracy [1,2]. Then we introduce a few simplifications which can be justified with the use of eikonal scattering waves, appropriate for high energy scattering. Finally, we apply the formalism to a detailed analysis of several observables which can be assessed in spectroscopic studies of rare nuclear isotopes probed with (p, pN) reactions in inverse kinematics.

II. QUASIFREE SCATTERING FORMALISM

A. Distorted wave impulse approximation

The standard DWIA expression for the quasifree cross section is [1,2]

$$\frac{d^3\sigma}{dT_N d\Omega'_p d\Omega_N} = K' \frac{d\sigma_{pN}}{d\Omega} |F(\mathbf{Q})|^2, \tag{1}$$

where K' is a kinematic factor, $|F(\mathbf{Q})|^2$ is the momentum distribution of the knocked-out nucleon N in the nucleus, and $d\sigma_{pN}/d\Omega$ is the free, or quasifree, pN cross section. In this formalism the off-shell pN t-matrix is required, and the factorized form that appears in Eq. (1) is valid only if off-shell effects are not very important. In proton-induced knock-out reactions at high energies this hypothesis has been confirmed in previous works [1,2].

B. Transition amplitude

In the DWIA, the transition amplitude for the $A(p, pN)B$ reaction is given by [1]

$$T_{p,pN} = \sqrt{S(lj)} \langle \chi^{(-)}_{\mathbf{k}'_p} \chi^{(-)}_{\mathbf{k}_N} | \tau_{pN} | \chi^{(+)}_{\mathbf{k}_p} \psi_{jlm} \rangle, \tag{2}$$

where $\chi^{(-)}_{\mathbf{k}'_p}$ ($\chi^{(-)}_{\mathbf{k}_N}$) is the distorted wave for an outgoing proton (knocked-out nucleon) in the presence of the residual nucleus B, $\chi^{(+)}_{\mathbf{k}_p}$ is the distorted wave for an incoming proton in the presence of the target nucleus A, and ψ_{jlm} is the bound state wave function of the knocked-out nucleon; $\sqrt{S(lj)}$ is the corresponding spectroscopic amplitude for a bound nucleon with quantum numbers (lj). Later, we will define the energy E at which the two-body pN scattering matrix τ_{pN} is evaluated.

In coordinate space the matrix element given by Eq. (2) can be written as

$$T_{p,pN} = \sqrt{S(lj)} \int d^3\mathbf{r}'_{pB} d^3\mathbf{r}'_{NB} d^3\mathbf{r}_{pA} d^3\mathbf{r}_{NB} \times \tau(\mathbf{r}'_{pB}, \mathbf{r}'_{NB}; \mathbf{r}_{pA}, \mathbf{r}_{NB}) \times \chi^{(-)*}_{\mathbf{k}'_p}(\mathbf{r}'_{pB}) \chi^{(-)*}_{\mathbf{k}_N}(\mathbf{r}'_{NB}) \chi^{(+)}_{\mathbf{k}_p}(\mathbf{r}_{pA}) \psi_{jlm}(\mathbf{r}_{NB}), \tag{3}$$

where the scattering waves are normalized so that

$$\int d^3\mathbf{r} \chi^*_{\mathbf{k}}(\mathbf{r}) \chi_{\mathbf{k}'}(\mathbf{r}) = \delta(\mathbf{k} - \mathbf{k}'),$$

and the bound-state wave function ψ_{jlm} is normalized to the unity,

$$\int d^3\mathbf{r} |\psi_{jlm}(\mathbf{r})|^2 = 1.$$

An inspection of the integrand in Eq. (3) can help us to eliminate several of the integrals. The coordinates of the proton and the nucleon N are related through $\mathbf{r}_{pA} = \mathbf{r}_{pN} + \mathbf{r}_{NA}$. Since the range of the pN interaction is much smaller than the nuclear size, the integral in Eq. (3) will sample small values of r_{pN} such that $r_{pN} \ll r_{NA}$. The T matrix in Eq. (3) reduces to an integral only over the $\mathbf{r}_{NB}$ coordinate [1,2],

$$T_{p,pN} = \sqrt{S(lj)} \tau(\mathbf{k}'_{pN}, \mathbf{k}_{pN}; E) \int d^3\mathbf{r}_{NB} \times \chi^{(-)*}_{\mathbf{k}'_p}(\mathbf{r}_{NB}) \chi^{(-)*}_{\mathbf{k}_N}(\mathbf{r}_{NB}) \chi^{(+)}_{\mathbf{k}_p}(\alpha \mathbf{r}_{NB}) \psi_{jlm}(\mathbf{r}_{NB}), \tag{4}$$

where $\alpha = (A-1)/A$ and $\tau(\mathbf{k}'_{pN}, \mathbf{k}_{pN}; E)$ is the Fourier transform of the pN t-matrix in Eq. (3).

The equation above has been the pillar of nearly all numerical calculations of quasifree $(p,2p)$ reactions. The factorization of the matrix element in Eq. (4) is exact in plane wave impulse approximation (PWIA). The argument used to justify it in DWIA is that the two-body interaction is of sufficiently short-range so that the distorted waves do not change significantly over the range which contributes significantly to the matrix element (3). Corrections to this approximation have been studied by several authors (see, e.g., [30]) and the results have been inconclusive in view of the several other approximations that have been further introduced.

Perhaps, the most serious approximation used to obtain Eq. (4) is the assumption of quasifree binary scattering, i.e., without the effects of multiple collisions, and other many-body effects such as antisymmetrization. The corrections due to these effects have been also reported in the literature, e.g., in Refs. [30,31]. The conclusions are that the deviations from the impulse approximation might be important, but they are also subject to uncertainty due to the use of several other approximations. We will thus retain the DWIA as our tool of choice, although we consider other corrections below. It should be emphasized that nonlocality corrections and spin-orbit terms in the optical potentials might play a relevant role and are not considered here. In Ref. [32] it was shown that the factorization approximation is valid for proton energies as low as 75 MeV. We will consider much higher energies here for which more simplifications can be done.

C. Cross section

The differential cross section is given by [33]

$$\frac{d^3\sigma}{dE'_p d\Omega'_p d\Omega_N} = \frac{K}{(2s_p+1)(2J_A+1)} \sum_\gamma |T_{p,pN}(\gamma)|^2, \tag{5}$$

where E'_p is the proton energy in the final channel, and the kinematical factor K is given by (here we use $k_i = p_i/\hbar$) [34]

$$K = \frac{m_p^2 m_N c^6}{(\hbar c)^6 (2\pi)^5} \frac{k'_p k_N}{k_p} \times \left| 1 + \frac{E_N}{M_B} \left[1 - \frac{k_p}{k_N} \cos\theta_N + \frac{k'_p}{k_N} \cos(\theta_p + \theta_N) \right] \right|^{-1}. \quad (6)$$

We define a *missing momentum*, $\mathbf{p}_m$, a *missing energy*, ϵ_m, and a *missing mass*, m_m, by means of

$$\begin{aligned} \epsilon_m &= E_N + E'_p - E_p - m_N, \\ \mathbf{p}_m &= \mathbf{k}_N + \mathbf{k}'_p - \mathbf{k}_p, \\ m_m^2 &= \epsilon_m^2 - p_m^2. \end{aligned} \quad (7)$$

The removal of the nucleon with momentum, p_m, from the nucleus implies a transfer of that three-momentum from the nucleus to the observed proton and knockout nucleon final state. For an exclusive reaction, only a small deficit in the final-state energy, ϵ_m can be observed.

The spin (projection) quantum numbers of the particle p and the target nucleus A in the initial state are $s_p(\mu_p)$ and $J_A(M_A)$, respectively. Also, in the final state the quantum numbers of the particles p and N and the residual nucleus B are $s_p(\mu'_p)$, $s_N(\mu_N)$, and $J_B(M_B)$, respectively. The summation (γ) of the transition matrix $T_{p,pN}$ in Eq. (5) is taken over the spin components

$$\gamma = (\mu_p, \mu'_p, \mu_N, M_A, M_B),$$

in the initial and final states. In the spin summation, the transition matrices will have an explicit dependence on $s_p(\mu_p, \mu'_p)$, $s_N(\mu_N)$, $J_A(M_A)$, and $J_B(M_B)$. Except for specific cases, we will use the simpler notation jlm for the angular momentum quantum numbers of the nucleons.

D. Plane wave impulse approximation

Physical insight is obtained by the use of the PWIA approximation, i.e., no scattering wave distortion. The relation between the pN scattering amplitude (in the pN c.m.) and the pN t-matrix is (see, e.g., [35])

$$f_{pN}(\theta; E) = -\frac{2\pi^2 m}{\hbar^2} \tau(\mathbf{k}'_{pN}, \mathbf{k}_{pN}; E), \quad (8)$$

in terms of which the (elastic) scattering cross section in the pN c.m. system is

$$\frac{d\sigma_{pN}}{d\Omega} = |f_{pN}(\theta; E)|^2. \quad (9)$$

If the wave functions in Eq. (4) are replaced by plane waves, one gets

$$T_{p,pN}^{(\mathrm{PWIA})} = \sqrt{S(lj)}\tau(\mathbf{k}'_{pN}, \mathbf{k}_{pN}; E) \int d^3\mathbf{r}\, e^{-i\mathbf{Q}.\mathbf{r}} \psi_{jlm}(\mathbf{r}), \quad (10)$$

where $\mathbf{Q}$ is the missing momentum defined in Eq. (7), and modified to

$$\mathbf{Q} = \mathbf{k}'_p + \mathbf{k}_N - \alpha \mathbf{k}_p, \quad (11)$$

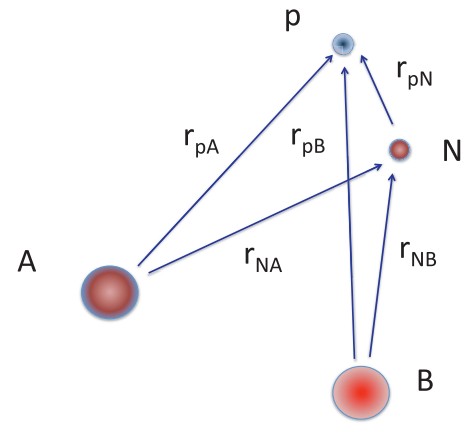

FIG. 1. (Color online) The coordinates used in the text are shown.

where we introduced a correction $\alpha = (A-1)/A$ to account for c.m. motion [1]. Thus, we reproduce Eq. (1), with

$$F(\mathbf{Q}) = \int d^3\mathbf{r}\, e^{-i\mathbf{Q}.\mathbf{r}} \psi_{jlm}(\mathbf{r}) \quad (12)$$

and the kinematic factor in Eq. (2) is given in terms of the kinematic factor of Eq. (5) as

$$K' = \left(\frac{\hbar^2}{2\pi^2 m} \right)^2 K. \quad (13)$$

Figure 1 show the coordinates used in the text.

Equation (10) is revealing: it tells us that in the lowest approximation, the $(p,2p)$ and (p,pn) cross sections are proportional to the momentum distribution of nucleons inside the target, determined by their wave function $\psi_{jlm}(\mathbf{r})$. This feature is common in many direct reactions as has been used in the identification and interpretation of many remarkable phenomena. For example, it has been used to identify "halo" structure in exotic nuclei [36], in the interpretation of momentum distributions in knockout reactions [3,37–49], or in the experimental analysis of transfer reactions, such as in the Trojan horse method for nuclear astrophysics [50–56].

Evidently, the PWIA is not a good approximation. In fact, distortions due to absorption and elastic scattering accounted for in DWIA lead to a deviation from Eq. (10) and its simple interpretation. But it is still useful for physical understanding of most results. Although $(p,2p)$ reactions have been carried out with high-energy protons, only rather recently, eikonal waves, and the Glauber treatment of multiple scattering have been used to account for distortions and absorption [25–29]. One probable reason is that measurements have been carried out for large angle scattering and sometimes large energy transfer, conditions that invalidate the use of the eikonal approximation, although attempts along these lines have been tried already at very early studies of $(p,2p)$ reactions [57,58]. We will show that the use of eikonal waves is still justified if care is taken to separate incoming and outgoing channels. The advantage of the eikonal formalism in comparison with traditional DWIA formalism as described in Refs. [1,2] is enormous because it allows a much easier treatment of the multiple-scattering problem.

E. Distorted waves

The PWIA approximation in Eq. (10) neglects important absorption and refraction properties of the nucleon scattering waves. In high-energy collisions, a much better result can be obtained by using the eikonal approximation

$$\chi_i(\mathbf{r})^{\text{in(out)}} = \exp\left[i\mathbf{k}_\mathbf{i}^{\text{in(out)}}\cdot\mathbf{r}\right] \times \exp\left[-\frac{i}{\hbar v}\int_{a_{\text{in(out)}}}^{b_{\text{in(out)}}} dz' U_i^{\text{in(out)}}(\mathbf{r}')\right], \quad (14)$$

where $\mathbf{r}\equiv(\mathbf{b},z)$, v is the velocity of the nucleon i and U_i is the optical potential accounting for all interactions of the particle with the nucleus. The integration limits are $a_{\text{in(out)}} = \mp\infty$ and the location where the collision occurs inside the projectile. An average of this position is done for each "impact parameter" b.

For practical purposes, one can also write Eq. (14) as

$$\chi_i(\mathbf{r})^{\text{in(out)}} = \mathcal{S}_{\text{in(out)}}(b)\exp\left[i\mathbf{k}_\mathbf{i}^{\text{in(out)}}\cdot\mathbf{r}\right], \quad (15)$$

with

$$\mathcal{S}_{\text{in(out)}}(b) = \exp\left[-\frac{i}{\hbar v}\int_{a_{\text{in(out)}}}^{b_{\text{in(out)}}} dz' U_i^{\text{in(out)}}(\mathbf{r}')\right]. \quad (16)$$

We can interpret $\mathcal{S}_{\text{in(out)}}(b)$ as the "*survival amplitudes*" for the incoming and outgoing waves. They measure the distortion and absorption of the incoming proton and outgoing nucleons as a function of their position in space.

For the real part of the optical potential, it is appropriate to use a microscopic folding potential, such as the M3Y [15] potential. The imaginary part of the optical potential, corresponding to reaction loss to other channels, needs to be introduced separately. For high energy collisions, this can be done by assuming that absorption is due to incoherent binary nucleon-nucleon collisions in the t-$\rho\rho$ approximation [35]. Then the optical potential entering Eq. (14) reads

$$U_i(\mathbf{r}) = U_i^{M3Y}(\mathbf{r}) + U_i^{(c)}(\mathbf{r}) - i\frac{E_i}{k_i}\sigma_i(E_i)\int \rho_{A(B)}(\mathbf{r}-\mathbf{r}')\rho_p(\mathbf{r}')d^3\mathbf{r}', \quad (17)$$

where $U_i^{(c)}$ is the Coulomb potential between the nucleon i and the nucleus A (entrance channel) or $B = A-1$ (outgoing channel). As the eikonal integral for the Coulomb field in Eq. (14) diverges, a regularized Coulomb phase is used [46]. The last term of Eq. (17) relates the imaginary part of the optical potential to the nucleon-nucleon cross section, which depends on the incoming proton, or outgoing nucleon, energy E_i. The integral contains the density of the nuclei A or B folded with the nucleon density. The intrinsic matter density of the proton (or neutron), $\rho_p(r)$, is taken as an exponential function, corresponding to a form factor $\rho_p(q) = (1+q^2/a^2)^{-1}$. We will use $a^2 = 0.71$ fm^{-2}, for a proton rms radius of 0.87 fm. The Fourier transforms for the nuclei A and B are obtained from theoretical nuclear densities, calculated by using Hartree-Fock + BCS theory according to Refs. [59,60].

F. Nucleon-nucleon cross sections

The free (total) nucleon-nucleon cross sections for $E >$ 10 MeV were fitted to the data of the Particle Data Group [61]. The fits are given by the expressions (1) and (2) of Ref. [62]. Their analytical fit reproduces very well the experimental total pp and pn cross sections in the energy interval 10 MeV $\leqslant E_{\text{lab}} \leqslant$ 5 GeV.

Medium corrections of the nucleon-nucleon cross sections can be relevant even at moderately high energies ($E_p \sim$ 200 MeV). At higher energies, nuclear transparencies can be nicely reproduced in Glauber calculations with free NN cross sections—very small medium corrections cannot be excluded, but the measured transparencies seem to indicate that they are small. In (p, pN) reactions the final proton or the knocked-out nucleon can have much lower energies than the incident proton, thus raising the importance of medium corrections. These corrections for nucleon-nucleon scattering in nuclear matter have been studied in, e.g., Refs. [62–69]. A calculation of medium effects using Brueckner-Hartree-Fock method shows that medium corrections are mainly due to Pauli blocking, which can be linked to functions of the local nucleon densities [69]. The analytical formulation developed in Refs. [62–64] yields the following parametrization for the nucleon-nucleus cross section in terms of the local nuclear density ρ (in fm^{-3}),

$$\sigma_{pN}(E_i,\rho) = \sigma_{pN}^{(\text{free})}(E_i)\left[1 - \frac{50.12\rho^{2/3}}{E_i} + \Theta\left(\frac{125.3\rho^{2/3}}{E_i} - 1\right) \times \frac{50.12\rho^{2/3}}{E_i}\left(1 - \frac{E_i}{125.3\rho^{2/3}}\right)^{5/2}\right], \quad (18)$$

where $\sigma_{pN}(E_i)$ is the free cross section, E_i is the nucleon laboratory energy in MeV, and Θ is the step function, i.e., $\Theta(x) = 0$ if $x < 0$, and $\Theta(x) = 1$ if $x > 0$. For an impact parameter b the above cross section is averaged along the incoming (outgoing) longitudinal coordinate z. This procedure yields the values of $\overline{\sigma_{pn}}$ and $\overline{\sigma_{pp}}$ to be used in Eq. (17). Further, the cross sections are averaged over the local number of protons and of neutrons (local isospin average). The nucleon-nucleon cross sections entering these expressions are given by

$$\overline{\sigma_p} = \frac{N_A}{A_A}\overline{\sigma_{pn}} + \frac{Z_A}{A_A}\overline{\sigma_{pp}}, \quad \overline{\sigma_{p'}} = \frac{N_B}{A_B}\overline{\sigma_{pn}} + \frac{Z_B}{A_B}\overline{\sigma_{pp}}, \quad \text{and} \quad \overline{\sigma_n} = \frac{N_B}{A_B}\overline{\sigma_{pp}} + \frac{Z_B}{A_B}\overline{\sigma_{pn}}, \quad (19)$$

where (N_A, Z_A, A_A) and (N_B, Z_B, A_B) are the neutron, charge, and mass numbers of the target and residual nucleus, respectively. A similar isospin average is used to obtain $\overline{\sigma_N}$, depending if the outgoing nucleon is $N =$ neutron or $N =$ proton.

III. MOMENTUM DISTRIBUTIONS

A. S matrices

Equation (14) allows a simple interpretation of the transition matrix for the scattering of a high energy projectile by a proton

in a (p, pN) reaction ($N = p$, or $N = n$, for proton or neutron knockout). We adopt a similar approach as in Refs. [37,38,40] for knockout reactions in nucleus-nucleus collisions. The two-body wave function for the incoming proton-nucleus channel is

$$\Psi_{\rm in} = \mathcal{S}_{\rm in} \exp(i\alpha \mathbf{k}_p \cdot \mathbf{r})\psi_{jlm}, \tag{20}$$

where $\mathcal{S}_{\rm in}$ is the scattering matrix (or survival amplitude) of the incoming proton up to the collision point and ψ_{jlm} is the single-particle wave function of the bound nucleon in its initial state. Analogously, the two-body wave function for the outgoing channel is given by

$$\Psi_{\rm out} = \mathcal{S}^{(p)}_{\rm out}\mathcal{S}^{(N)}_{\rm out} \exp[i(\mathbf{k}_N + \mathbf{k}'_p) \cdot \mathbf{r}], \tag{21}$$

where $S^i_{\rm out}$ is the scattering matrices (survival amplitudes) for the outgoing nucleon $i = p$ (proton) or N (knocked-out nucleon). The scattering matrices (survival amplitudes) account for the distortions in the incoming and outgoing channels, as well as for the absorption in those channels. Absorption means that if other binary collisions occur, other channels will open and the contribution to the (p, pN) channel will be lost. Absorption is taken care of by the last term of Eq. (17). Note that in separating the scattering into an incoming and outgoing wave, the conditions of validity of the eikonal approximation, Eq. (14), are satisfied, as long as the deviations from a straight-line during the incoming and, separately, during the outgoing channels, are kept small. The energy loss along these paths in both channels is also expected to be small, the main energy transfer occurring during the quasifree p, pN scattering.

The interpretation of the (p, pN) reaction is now straightforward. The transition matrix is simply given by

$$T^{(eik)}_{p,pN} = \sqrt{S(lj)}\, \tau(\mathbf{k}'_{pN}, \mathbf{k}_{pN}; E)\langle \Psi_f | \Psi_i \rangle,$$

where $\sqrt{S(lj)}$ is the amplitude to find the bound nucleon in the orbital jlm, $\tau(\mathbf{k}'_{pN}, \mathbf{k}_{pN}; E)$ is the proton-nucleon scattering amplitude, and $\langle \Psi_f | \Psi_i \rangle$ are overlap integrals of the initial and final states of the nuclei $A \to B$. In an independent particle model with a spectator nucleus B one can write that $\langle \Psi_f | \Psi_i \rangle \approx \langle \Psi_{\rm out} | \Psi_A \rangle$. Apart from kinematical factors, the total scattering amplitude is the product of the free nucleon-nucleon scattering amplitude times the probability amplitude for finding inside the nucleus a nucleon at position $\mathbf{r}$. The equation above can also be rewritten as

$$T^{(eik)}_{p,pN} = \sqrt{S(lj)}\tau(\mathbf{k}'_{pN}, \mathbf{k}_{pN}; E) \int d^3\mathbf{r}\, e^{-i\mathbf{Q}.\mathbf{r}} \mathcal{S}(b, \theta)\psi_{jlm}(\mathbf{r}), \tag{22}$$

where $\mathbf{Q}$ is given by Eq. (11), $\theta \equiv \theta(\theta'_p, \theta_N)$ is a function of the angles θ'_p and θ_N, and $\mathcal{S}(b, \theta)$ is the product of scattering matrices for pA, $p'B$, and NB scattering, i.e.,

$$\mathcal{S}(b, \theta) = \mathcal{S}_{pA}(E_p, b)\mathcal{S}_{p'B}(E'_p, \theta'_p, b)\mathcal{S}_{NB}(E_N, \theta_N, b), \tag{23}$$

with the scattering matrices for the initial proton-target (pA), the final proton-residual nucleus (pB), and the nucleon-residual nucleus (NB) scattering.

The semi-inclusive differential scattering cross section for the reaction $A(p, pN)B$ by removing a nucleon from the orbital jl under conditions of fixed $\mathbf{Q}$ is given by

$$d\sigma = \frac{d^3Q}{(2\pi)^3}\frac{1}{2j+1}\left(-\frac{2\pi^2 m_p}{\hbar^2}\right)^2 \sum_m |T^{(eik)}_{p,pN}|^2, \tag{24}$$

where $d^3\mathbf{Q}/(2\pi)^3$ is the density of states and the sum takes care of the average over all magnetic substates of the bound-state wave function ψ_{jlm}. In the last equality, we have made use of the Eq. (8).

We perform an average of $d\sigma_{pN}/d\Omega$ and the scattering matrices over all possible energies of the final proton and nucleon which lead to the momentum transfer Q. Hence, our differential cross section in the distorted wave impulse approximation (DWIA) is given by

$$\left(\frac{d\sigma}{d^3Q}\right)_{\rm DWIA} = \frac{1}{(2\pi)^3}\frac{S(lj)}{2j+1}\sum_m \left\langle \frac{d\sigma_{pN}}{d\Omega}\right\rangle_Q \times \left| \int d^3\mathbf{r}\, e^{-i\mathbf{Q}.\mathbf{r}} \langle \mathcal{S}(b)\rangle_Q \psi_{jlm}(\mathbf{r})\right|^2. \tag{25}$$

Here the S matrix is also averaged over all pp′ scattering angles leading to the same magnitude of the momentum transfer Q. Equation (25) is our starting formula for the calculations of the momentum distributions of the recoiled fragments.

We neglect the fact that the momenta of the quasifree matrix element do not occur in the free scattering because of the difference in energy conservation between the two cases. This difference is caused by the nonzero value of the separation energy in the quasifree scattering and by the energy and momentum carried by the recoiling nucleus. In other words, $d\sigma_{pN}/d\Omega$ in Eq. (24) is a half-off-the-energy-shell cross section. In non-relativistic terms, the off-shellness is because energy conservation in the $(p, 2p)$ or (p, pn) vertex receive corrections of the form $-S_N + p_m^2/2M_B$, where p_m is the missing momentum, or recoil momentum of nucleus $B = A - 1$ given by Eq. (7) and S_N is the nucleon separation energy. Due to this mismatch, there is a certain arbitrariness in chosing the value of $d\sigma_{pN}/d\Omega$ in Eq. (1). This is an amount $S_N + p_m^2(1/m_N - 1/M_B)/2$ off shell. The importance of off-energy-shell effects has been investigated in Refs. [12,70,71]. The conclusion is that off-energy-shell effects are small and can be neglected. Thus, the standard prescription is to replace $d\sigma_{pN}/d\Omega$ by the measured on-energy-shell cross section, i.e., the elastic pN scattering. This approximation amounts only to a few percent uncertainty as long as one considers quasifree processes for proton energies greater than 200 MeV [1,72].

The free $d\sigma_{pN}/d\Omega$ cross section shows a considerable anisotropy in the laboratory energy range of $E_p =$ 200–1000 MeV. Phase-shift analyses of pp and pn elastic scattering cross sections are available (e.g., Refs. [73,74]), yielding elaborate parametrizations that are generally in good agreement with the data [75]. We take into account the angular anisotropy and the parametrizations by using a fit to the experimental differential nucleon-nucleon cross sections as explained in Ref. [75]. The angular distributions were obtained using the computer code SAID, which implements a comprehensive phase-shift analysis that encompasses the world elastic pp and pn scattering data [74].

B. Single particle wave functions

If the nuclear states are assumed to be independent on the total angular momentum of the residual nucleus, one can write

$$\psi_{jlm} = \frac{u_{lj}(r)}{r} \sum_{m_l\, m_s} \langle l m_l s m_s | j m \rangle Y_{l m_l}(\widehat{\mathbf{r}}) \chi_{m_s}, \tag{26}$$

where $\langle l m_l s m_s | j m \rangle$ are Clebsch-Gordan coefficients, $Y_{l m_l}$ are spherical harmonics, and χ_{m_s} are spinors. The radial wave function is normalized so that $\int dr |u_{lj}(r)|^2 = 1$. These wave functions are calculated using a Woods-Saxon potential with central, surface, and spin-orbit parts (see, e.g., [46]). The integral in Eq. (25) has cylindrical symmetry which can be exploited for practical purposes to reduce it to a double-fold integral (on b and z, if the wave function has spherical symmetry). In this case one gets

$$\begin{aligned} G(\mathbf{Q}) &= \int d^3\mathbf{r}\, e^{-i\mathbf{Q}.\mathbf{r}} \langle \mathcal{S}(b) \rangle_Q \psi_{jlm}(\mathbf{r}) \\ &= 2\pi \int_0^\infty db\, b \langle \mathcal{S}(b) \rangle_Q \int_{-\infty}^\infty dz \exp[-i Q_z z] \frac{u_{lj}(r)}{r} \\ &\quad \times \sum_{m_l\, m_s} (-i)^{m_l} \mathcal{C}_{l m_l} J_{m_l}(Q_t b) \langle l m_l s m_s | j m \rangle \\ &\quad \times P_{l m_l}(\cos\vartheta) \chi_{m_s}, \end{aligned} \tag{27}$$

where Q_t and Q_z are the transverse and longitudinal projections of $\mathbf{Q}$ along and perpendicular to the beam direction, $r = \sqrt{b^2 + z^2}$ and $\cos\vartheta = z/\sqrt{b^2 + z^2}$. The inclusion of the spinors χ_{m_s} imply $|G(\mathbf{Q})|^2 \equiv G^\dagger G = |G_-|^2 + |G_+|^2$, where G_- is the spin-down and G_+ the spin-up amplitude. In the second equality we made use of the fact $Y_{lm}(\vartheta, 0) = C_{lm} P_{lm}(\cos\vartheta)$, where P_{lm} are the Legendre polynomials, and

$$\mathcal{C}_{lm} = (-1)^m \sqrt{\frac{2l+1}{4\pi}} \sqrt{\frac{(l-m)!}{(l+m)!}}.$$

$J_m(x)$ are cylindrical Bessel functions.

As a function of the total momentum $\mathbf{Q}$, another useful expression for $G(\mathbf{Q})$ is

$$\begin{aligned} G(\mathbf{Q}) &= 4\pi i^l \sum_{m_l\, m_s} i^{m_l} \langle l m_l s m_s | j m \rangle Y_{l m_l}(\widehat{\mathbf{Q}}) \chi_{m_s} \\ &\quad \times \int dr\, r\, j_l(Qr) \langle \mathcal{S}(r) \rangle_Q u_{lj}(r), \end{aligned} \tag{28}$$

where $j_l(x)$ is the spherical Bessel function.

C. Cross sections

Using the orthogonality relation of the spherical harmonics, we can integrate Eq. (25) to get the *total momentum distribution*

$$\begin{aligned} \frac{d\sigma}{Q^2 dQ} &= \frac{2}{\pi} \frac{S(lj)}{2j+1} \left\langle \frac{d\sigma_{pN}}{d\Omega} \right\rangle_Q \\ &\quad \times \left| \int_0^\infty dr\, r \langle \mathcal{S}(r) \rangle_{Q_z} j_l(Qr) u_{lj}(r) \right|^2. \end{aligned} \tag{29}$$

Using the relation

$$\int_0^{+\infty} x J_m(\alpha x) J_m(\beta x) dx = \frac{1}{\alpha} \delta(\alpha - \beta), \tag{30}$$

we can integrate $|G(\mathbf{Q})|^2$ over Q_t using Eq. (27) and we obtain the *longitudinal momentum distribution*,

$$\begin{aligned} \frac{d\sigma}{dQ_z} &= \frac{S(lj)}{2j+1} \sum_m \left\langle \frac{d\sigma_{pN}}{d\Omega} \right\rangle_{Q_z} |\mathcal{C}_{lm}|^2 \\ &\quad \times \int_0^\infty db\, b \left| \langle \mathcal{S}(b) \rangle_{Q_z} \right|^2 \\ &\quad \times \left| \int_{-\infty}^\infty dz \exp[-i Q_z z] \frac{u_{lj}(r)}{r} P_{lm}(b, z) \right|^2. \end{aligned} \tag{31}$$

Using the relation

$$\frac{1}{2\pi} \int \exp[i(\alpha - \beta)x] dx = \delta(\alpha - \beta), \tag{32}$$

we can integrate $|G(\mathbf{Q})|^2$ over Q_z using Eq. (27) and we obtain the *transverse momentum distribution*,

$$\begin{aligned} &\frac{d\sigma}{Q_t dQ_t} \\ &= \frac{S(lj)}{2j+1} \sum_m \left\langle \frac{d\sigma_{pN}}{d\Omega} \right\rangle_{Q_t} |\mathcal{C}_{lm}|^2 \int_{-\infty}^\infty dz \\ &\quad \times \left| \int_0^\infty db \langle \mathcal{S}(b) \rangle_{Q_t} \frac{u_{lj}(r)}{r} J_m(Q_t b) P_{lm}(b, z) \right|^2. \end{aligned} \tag{33}$$

The *total cross section* is obtained either from integrations of Eq. (31) or of Eq. (33), using the closure relations (30) or (32). One obtains

$$\begin{aligned} \sigma &= S(lj) \frac{2\pi}{2j+1} \sum_m \left\langle \frac{d\sigma_{pN}}{d\Omega} \right\rangle_{o.s.} |\mathcal{C}_{lm}|^2 \\ &\quad \times \int_0^\infty db\, b |\langle \mathcal{S}(b) \rangle_{o.s.}|^2 \int_{-\infty}^\infty dz \left| \frac{u_{lj}(r)}{r} P_{lm}(b, z) \right|^2. \end{aligned} \tag{34}$$

The subscript "*o.s.*" in the above equation means that an average over the final momenta is made, which satisfies the on-shell conservation of energy for a nonrelativistic nuclear recoil energy, as described in Eq. (7). In practice, the average is done by a Monte Carlo sampling of the differential cross sections for several final momenta $\mathbf{k}'_p$ and $\mathbf{k}_N$ with the constraint set by conservation of energy and momentum,

$$\left\langle \frac{d\sigma_{pN}}{d\Omega} \right\rangle_{o.s.} = \frac{\int_{\mathbf{k}'_p, \mathbf{k}_N \in (o.s.)} d^3\mathbf{k}'_p d^3\mathbf{k}_N \frac{d\sigma_{pN}}{d\Omega}}{\int_{\mathbf{k}'_p, \mathbf{k}_N \in (o.s.)} d^3\mathbf{k}'_p d^3\mathbf{k}_N}. \tag{35}$$

For the momentum distributions obtained with Eqs. (29), (31), and (33) the average is done with the constraint set by the total momentum Q, while for the total cross section, the constraint $Q = 0$ is used for simplicity.

Equation (34) allows us to define a *nucleon knockout probability* at a given impact parameter b by means of

$$P(b) = \frac{S(lj)}{2j+1} \sum_m \left\langle \frac{d\sigma_{pN}}{d\Omega} \right\rangle_{o.s.} |\mathcal{C}_{lm}|^2 |\langle \mathcal{S}(b) \rangle_{o.s.}|^2 \times \int_{-\infty}^{\infty} dz \left| \frac{u_{lj}(r)}{r} P_{lm}(b,z) \right|^2. \quad (36)$$

This equation is useful to calculate the parts of the transverse coordinate b of the single-particle wave function which is probed by the nucleon knockout mechanism.

The knockout of a nucleon will often lead to a state of short lifetime, which might decay to other channels than (p, pN). If, for example, an $0s_{1/2}$ proton from a nucleus like carbon has been knocked out, the Pauli principle no longer excludes those nuclear state rearrangements in which a p-shell proton falls into the hole of the s shell ejecting another particle from the nucleus. This decay energy can also be shared among all nucleons forming a compound nuclear state which later decays by particle evaporation. For simplicity we will not consider these situations in this work, leaving it for future analysis.

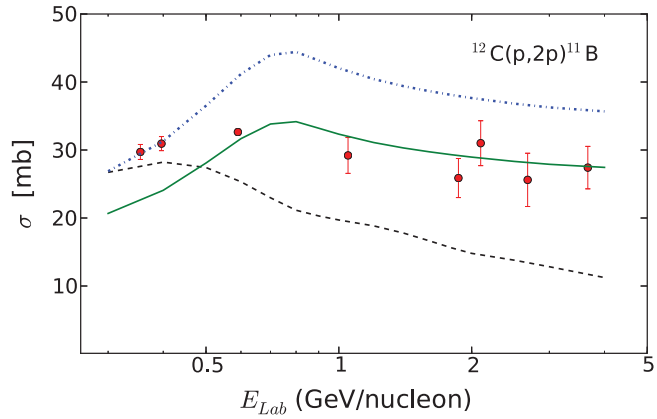

FIG. 2. (Color online) Cross sections of $^{12}C(p,2p)^{11}B$ fragmentation on hydrogen targets. The data are from Refs. [76,77]. The dashed-dotted curve shows the cross section calculated according to Eq. (34), with $\langle d\sigma_{pp}/d\Omega \rangle_{o.s.} = \sigma_{pp}^{tot}/4\pi$ where σ_{pp}^{tot} is total p-p free cross section. The full curve shows the same calculation multiplied by a factor 0.77. The dashed curve uses $\langle d\sigma_{pp}/d\Omega \rangle_{o.s.}$ given by the angular average of the *elastic pp* cross section satisfying the energy constraint of Eq. (7).

IV. RESULTS

Before we discuss $(p,2p)$ and (p,pn) reactions with unstable nuclei, we will establish how well the formalism described above reproduces quasifree knockout reactions on stable targets. The ingredients for the calculations are the equations developed above plus (a) total nucleon-nucleon cross sections, using the fit of Ref. [62], (b) elastic differential cross sections, using the Nijmegen global fit of the *NN* database [74], (c) nuclear densities calculated with the Hartree-Fock-Bogoliubov method, (d) single-particle wave functions calculated with a Woods-Saxon + spin orbit potential with parameters chosen to reproduce the separation energies, and (e) spectroscopic factors. According to Eq. (34), total cross sections in (p, pN) reactions are directly related to spectroscopic factors. On the other hand, momentum distributions should depend on the angular momentum of the single-particle state probed in the reaction, according to Eqs. (29), (31), and (33). Unless stated otherwise, we use spectroscopic factors equal to the unity for the sake of concentrating on the dependence on other physical inputs in the calculations.

A. Stable nuclei

1. Cross sections

In Fig. 2 we show the cross sections for $^{12}C(p,2p)^{11}B$ fragmentation on hydrogen targets compared to experimental data. We consider p (s) states in ^{12}C with proton separation energies of 15.9 (30.8) MeV and neutron separation energies of 18.7 (35.1) MeV, respectively. The dashed curve is a calculation using Eq. (34) and $\langle d\sigma_{pp}/d\Omega \rangle_{o.s.}$ given by the angular average of the *elastic pp* cross section satisfying the energy constraint of Eq. (7). For comparison purposes we also show by a dashed-dotted curve the cross sections calculated assuming $\langle d\sigma_{pp}/d\Omega \rangle_{o.s.} = \sigma_{pp}^{tot}/4\pi$ where σ_{pp}^{tot} is the total p-p free cross section. In both cases the calculated cross sections fail to reproduce the experimental data. By using the total p-p cross section one also includes pion production which is likely to leave behind an excited fragment. One naturally expects that it will overestimate the value of the $^{12}C(p,2p)^{11}B$ as compared to the experimental data. The full curve is the same as the dashed-dotted curve, but multiplied by a factor 0.77. It shows a better agreement with the data. A rescaling by any factor would not bring the dashed curve to a good agreement with the experimental data.

Our calculations are done assuming the knockout from p states only. Since the s-hole states are produced with high excitation energies, other particles are expected to be emitted from the decay, leading to a small contribution to the (p, pN) channel [10].

In Fig. 2 one observes a decrease of the calculated cross section as the bombarding energy decreases below $E_{\rm lab} \lesssim$ 700 MeV/nucleon. This is attributed to the fact that a sizable fraction of the scattered and knocked-out protons have an energy below 200 MeV. At these energies and below, the proton mean-free path is considerably reduced because the nucleon-nucleon cross sections rapidly increase as their relative energy decreases. A model similar to ours, containing many simplifying assumptions, was published in Ref. [89]. They have also used as input the total $\langle d\sigma_{pp}/d\Omega \rangle_{o.s.} = \sigma_{pp}^{tot}/4\pi$, with σ_{pp}^{tot} being the p-p total cross section. Their results have a better agreement with other experimental data [89] than ours. The reason for their successful results is puzzling as their model contains many more simplifying assumptions than ours.

The calculation using *elastic* p-p differential cross sections, with an average over the possible scattering angles, is shown by a dashed line in Fig. 2. It is very common in the literature to find calculations using $\langle d\sigma_{pp}/d\Omega \rangle_{o.s.} = (d\sigma_{pp}/d\Omega)^{\rm elast}_{\theta_{\rm c.m.}=90^\circ}$. In our calculations we use the constraints set by the energy-momentum conservation laws, which allows for scattering

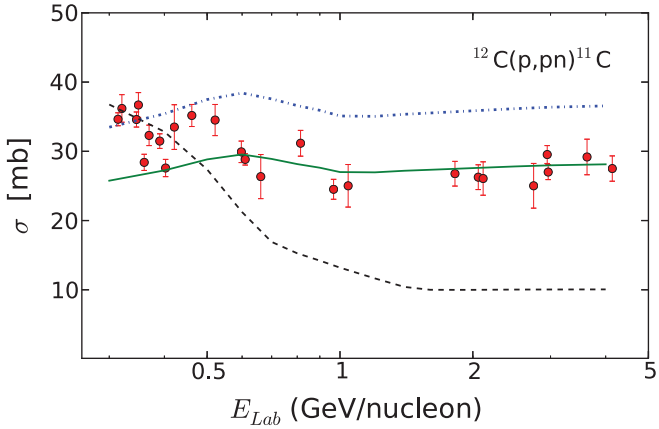

FIG. 3. (Color online) Cross sections of ^{12}C(p, pn)^{11}C fragmentation on hydrogen targets. The data are from Refs. [76–88]. The dashed-dotted curve shows the cross section calculated according to Eq. (34), with $\langle d\sigma_{pn}/d\Omega\rangle_{o.s.} = \sigma_{pn}^{\rm tot}/4\pi$ where $\sigma_{pn}^{\rm tot}$ is total p-n free cross section. The full curve shows the same calculation multiplied by a factor 0.77. The dashed curve uses $\langle d\sigma_{pn}/d\Omega\rangle_{o.s.}$ given by the angular average of the *elastic* p-n cross section satisfying the energy constraint of Eq. (7).

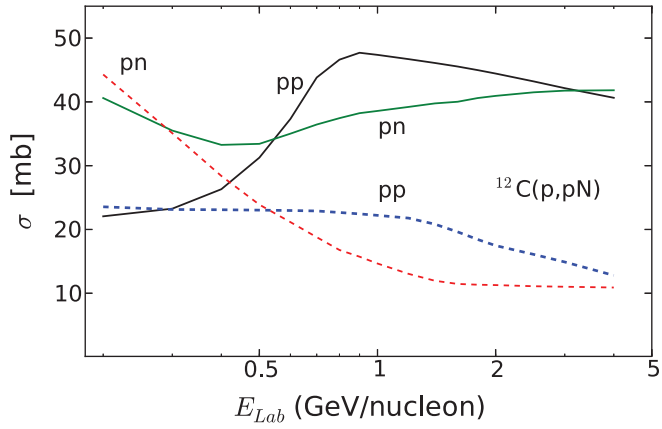

FIG. 4. (Color online) Free p-p and p-n *total* cross sections (solid curves) as compared to the constrained angle averaged *elastic* p-p and p-n cross sections (dashed curves) according to Eq. (35) and for ^{12}C(p, pN), with $N = p$ or n.

angles close to but not restricted to this value. The $(p, 2p)$ cross sections calculated with elastic cross sections lie consistently below the experimental data for $E_{\rm lab} \gtrsim 500$. And they deviate more from the experimental data with increasing bombarding energy. In fact, the elastic p-p cross section becomes increasingly smaller than $\sigma_{pp}^{\rm tot}$ at energies beyond 500 MeV/nucleon [90]. At these energies, the p-p angular distribution is also more and more anisotropic, showing a dip at c.m. scattering angles around 90°. Hence, the averaged p-p elastic cross sections include larger scattering angles, with outgoing protons being more strongly absorbed and with smaller scattering cross sections.

Similar features are seen our calculations presented in Fig. 3 for ^{12}C(p, pn)^{11}C as a function of the bombarding energy. Here the deviations obtained with the elastic p-n cross sections are more accentuated from those with isotropic *total* nucleon-nucleon cross sections than for the ^{12}C$(p, 2p)^{11}$B reaction (Fig. 2). One obvious reason is that the p-n elastic angular distributions is more asymmetric than in the p-p case. At the lower energies, additional cross section from excitation of giant resonances (GRs) might contribute more, deserving further investigation.

In Fig. 4 we show the free p-p and p-n *total* cross sections (solid curves) as compared to the constrained angle averaged *elastic* p-p and p-n cross sections (dashed curves) according to Eq. (35) and for ^{12}C(p, pN), with $N = p$ or n. Not all scattering angles are possible when the energy-momentum conditions in Eq. (7) are met. It is clear that the constrained angle averaged elastic cross sections are in most part responsible for the differences shown in Figs. 2 and 3 between the knockout cross sections obtained with total and with elastic nucleon-nucleon cross sections. The other part responsible for the differences is due to absorption effects generated by multiple binary collisions at different scattering angles. One observes in the figure that the medium averaged elastic cross sections (dashed curves) are smaller than the respective total free NN cross sections, as expected. However this difference decreases with decreasing energy and at energies below 300 MeV the elastic, medium averaged, cross sections become larger than the free total NN cross sections. This arises because absorption due to multiple scattering in the medium favors scattering angles away from 90° where the differential cross section has a minimum. Hence, the averaged total elastic cross sections are larger than they would be without medium corrections because the largest values of the elastic differential cross section weight more on the average.

One of the main issues related to the (p, pN) cross sections at high energies (∼1 GeV) is to separate the different contributions arising from collective excitations leading to energy loss and to evaporation, and binary scattering with and without pion production. As shown from direct experimental analysis (see, e.g., Ref. [91]), the (p, pN) cross section gets contributions from (a) nucleon-nucleon quasielastic scattering, (b) nucleon-nucleon inelastic scattering, and (c) a low excitation energy. The cross sections, for all three cases are comparable. The shapes of the momentum distributions in cases can be reproduced with a nucleon-nucleon cascade model including pion production, but the theoretical predictions for the quasielastic component is too large by a factor of 3 [91]. The low momentum transfer peak is consistent with two mechanisms: (1) an excitation and decay via proton emission of the carbon projectile and (2) a projectile proton scattering diffractively off the C target. Finally, the Fermi momentum determined from the transverse momentum distribution is 160 ± 11 MeV/c compared to 190 ± 11 MeV/c from the longitudinal momentum distribution.

We thus conclude that a direct comparison of our calculations with experimental data as shown in Figs. 2 and 3 is hampered by the fact that the data are inclusive. A kinematically complete measurement of quasielastic scattering including the selection of the quasifree kinematical condition would allow a direct comparison with the calculated cross section using the elastic nucleon-nucleon cross section as an input. However, such data have been measured so far

only with very restricted angular acceptances. The analysis of Webb *et al.* [91] shows that only around 50% of the inclusive cross section at 1 GeV/nucleon corresponds to quasielastic scattering. The cross section measured by those authors is 8.8(2.5) mb compared to our prediction of about 20 mb using elastic $d\sigma_{pp}/d\Omega$ at 1 GeV. The reduction by 0.44(13) is to be compared to the usual reduction factor 0.6 from $(e, e'p)$ experiments. The experimental cross section in Ref. [91] has been acceptance corrected using the cascade model, meaning that it is model dependent. The fully exclusive experiments in inverse kinematics as planned at the radioactive-beam facilities [8–11] will provide a full solid-angle coverage, and will thus be directly comparable to our predictions.

The features described in Figs. 2 and 3 have also been observed for several other $(p, 2p)$ and (p, pn) in our studies. In the literature one finds experimental (p, pN) cross sections well described by means of phenomenological parameter fitting models, such as those presented in Refs. [79,92]. The cross sections are also well described with microscopic theoretical models such as that reported in Ref. [89] where total nucleon cross sections for Eq. (35) were used and an analytical formulation for the (p, pN) reaction was given, with further approximations. We are not certain what physics input in such models validate their use and allow for a better agreement with the data.

Other common approximations found in the literature are (a) replacing $\langle d\sigma_{pN}/d\Omega\rangle_{o.s.}$ by the *total* free nucleon-nucleon cross section at 90° and keeping the same value for all bombarding energies (see, e.g., Refs. [1,35,93]), and (b) using phenomenological effective nucleon-nucleon interactions fitted to other nucleus-nucleus collision processes (such as charge-exchange reactions), instead of nucleon-nucleon cross sections (see, e.g., Ref. [94]). The use of Glauber theory was also recognized as an important theoretical tool to treat multiple scattering as well as to formulate a relativistic covariant model (see, e.g., Refs. [25–28]). On the other hand, the use of Mandelstam variables has proven to have the advantage of relating theoretical values to detection efficiencies in high-energy collisions [95] in a more straightforward way. This approach has been used in Ref. [96] to study quasifree α knockout from ^{6,8}He beams with a relative success.

It is also evident from Figs. 2 and 3 that the experimental data at energies of the order of 200–500 MeV are rather well described by using either total or elastic nucleon-nucleon cross sections. In fact, the total elastic and total inelastic nucleon-nucleon cross sections in free space have nearly the same values at this energy range. The differential elastic cross sections tend to be more asymmetric at larger energies. We therefore conclude that this energy range should be best suitable for studies of (p, pN) reactions.

In Fig. 5 we plot the proton and neutron knockout probabilities from p states in ^{12}C using Eq. (36). The solid curves are for (p, pn) and dashed curves for $(p, 2p)$. We also show the results obtained with $\langle \mathcal{S}(b)\rangle_{o.s.} = 1$ in Eq. (36). This would correspond to a direct NN knockout, without multiple binary collisions (no rescattering). In this case the knockout probabilities are very large, almost violating unitarity. Absorption due to knockout reduces the one-nucleon knockout probability considerably, as can be seen by the lower curves.

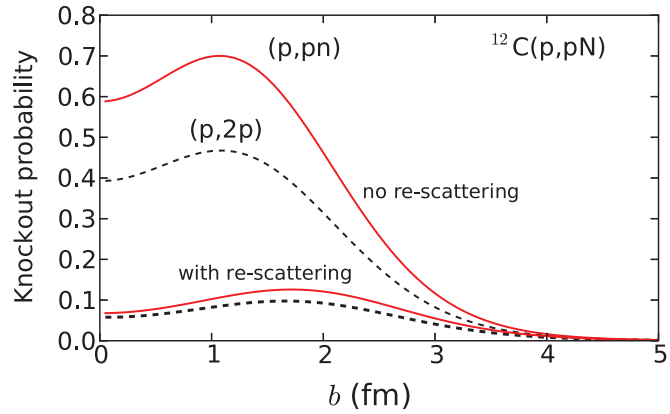

FIG. 5. (Color online) Proton and neutron knockout probabilities from p states in ^{12}C at 500 MeV/nucleon, according to Eq. (36). The solid curves are for (p, pn) and dashed curves for $(p, 2p)$. We also show the results obtained with $\langle \mathcal{S}(b)\rangle_{o.s.} = 1$ in Eq. (36) (no rescattering).

There is a larger reduction at smaller impact parameters than at the surface, as expected from basic principles. From central collisions ($b = 0$) there is a larger reduction due to absorption from the one-nucleon knockout channel. For collisions at low impact parameters we find an average reduction by a factor 6.8 for $(p, 2p)$ reactions and by a factor 8.7 for (p, pn) reactions.

Multiple scattering effects have been studied by several authors, using the Feshbach-Koonin-Kawai formalism (see, e.g., Refs. [97–106]), or the multiple scattering Glauber formalism (see, e.g., Refs. [25–28]), or even with a simple one parameter rescaling factor model (see, e.g., Refs. [1,89]). It is clear however that the effects of multiple scattering are very large and need to be taken into account carefully if the total cross section is supposed to be useful for the purposes of extracting spectroscopic factors.

A simple approximation for dealing with the effects of multiple scattering is to assume that the central probability scales as

$$P \simeq P_0 \exp\left[-\frac{3R}{\lambda}\right], \tag{37}$$

where P_0 is the probability without absorption, R is the nuclear radius, and λ is the nucleon mean free path. The factor 3 in the numerator is due to the three particles; one in the incoming channel and two in the outgoing channel. We use $R = 2.6$ fm, corresponding to the mean square radius of ^{12}C. This yields a mean free path for protons in ^{12}C of about $\lambda \simeq 2.9$ fm at 800 MeV/nucleon. Despite the approximations used for this estimate, this result is remarkably close to the mean-free path of high-energy protons in ^{12}C, $\lambda \simeq 2.4$ fm, deduced in Ref. [107].

2. *Momentum distributions*

In nucleon knockout in heavy-ion reactions, momentum distributions are known to be a useful probe of the angular momentum of the knocked-out nucleon. Due to the centrifugal barrier, a state with large l is confined to a smaller region,

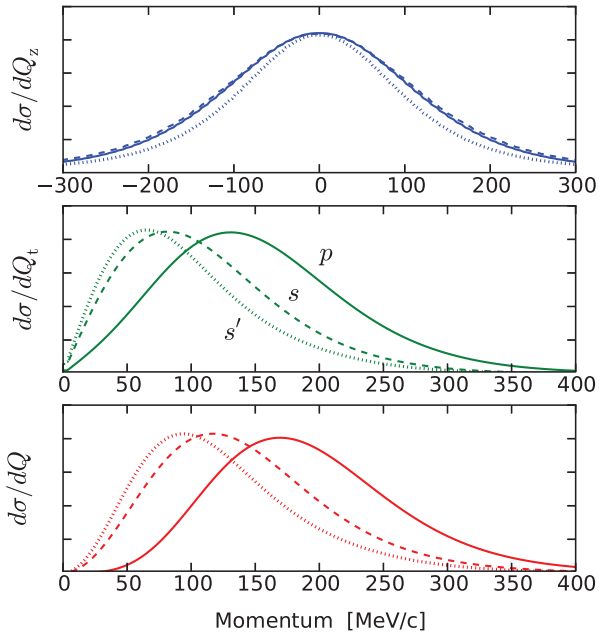

FIG. 6. (Color online) Longitudinal (upper panel), transverse (middle panel), and total momentum distributions (lower panel) for the missing momentum in ^{12}C$(p, 2p)^{11}$B fragmentation on hydrogen targets. The full curves are for p states, the dashed curves are for s states. The dotted curves s' correspond to the calculations where the energy of the s states are taken as the p-state energy. The curves are rescaled to be shown in the same plot.

yielding a broader momentum distribution [40]. The separation energy is also an important factor to determine the size of the bound-state single-particle function and has been a useful tool to uncover the existence of unstable halo nuclei [36]. In our calculations, the proton p-state energy in ^{12}C is set to the proton separation energy, i.e., $\epsilon_p = -15.9$ MeV and the s-state energy to $\epsilon_s = -30.8$ MeV.

In Fig. 6 we show the longitudinal (upper panel), transverse (middle panel), and total momentum distributions (lower panel) for the missing momentum, Eq. (7), in ^{12}C$(p, 2p)^{11}$B reactions on hydrogen targets at 500 MeV/nucleon. The full curves are for p states, the dashed curves are for s states. The dotted curves s' correspond to calculations for which the energy of the s states are taken as the same energy as the p-state energy. We have normalized the curves to a peak value as we are only interested in the variation of the widths of the distributions with the energy and angular momentum of the involved single-particle orbitals.

Two effects are competing in the calculations of the p-state and s-state proton removal shown by the solid and dashed curves in Fig. 6. On the one hand, the l dependence widens the distribution for the p states compared to those for the s states. On the other hand, the separation energy of the s state being larger than that for the p state compensates by widening the s-state contribution. The transverse and total momentum distributions (middle and lower panels) are still able to discern between the two states. But for the longitudinal momentum distributions the two curves are almost identical in shape. When the energy of the s state is artificially set equal to the energy of the p state, the shape of the s- and p-momentum distributions differ substantially. It is clear that the momentum distributions displayed either in terms of transverse, or total missing momentum, are a sensitive probe of the angular momentum state of the orbital from which the proton is removed. A similar conclusion was obtained in $(e, e'p)$ momentum distribution analyses [108].

B. Neutron rich nuclei

The prominent differences between stable and neutron-rich unstable nuclei are: (a) extended neutron distribution in the form of a halo, or skin, and (b) smaller binding energies than those for stable nuclei. Here we will explore both cases and their imprints in the cross sections and momentum distributions in $(p, 2p)$ and (p, pn) reactions.

1. Cross sections

As an example for the dependence of the cross sections on the separation energy, we consider (p, pn) reactions with ^{23}O, with valence neutrons in the $[0d_{5/2}]^6\,[1s_{1/2}]$ configuration. The separation energies are $S_n(1s_{1/2}) = 2.73$ MeV and $S_n(0d_{5/2}) = 6.0$ MeV. We artificially vary the separation energy of theses states to explore the separation energy dependence of the (p, pn) cross sections at 500 MeV/nucleon.

In Fig. 7 we plot the cross sections for neutron removal in (p, pn) reactions on ^{23}O from $[0d_{5/2}]^6$ and $[1s_{1/2}]$ orbitals as a function of the separation energy. The cross sections for neutron removal from the $[0d_{5/2}]^6$ orbital is divided by the number of the neutrons in the orbital (6). As expected, the cross sections are strongly energy dependent close to the threshold and steadily decrease with increasing separation energy. Close to threshold (i.e., close to $S_n = 0$) a large chunk of the wave function lies in a region where absorption, or multiple scattering, is smaller, thus increasing the removal probability at larger impact parameters, consequently increasing the

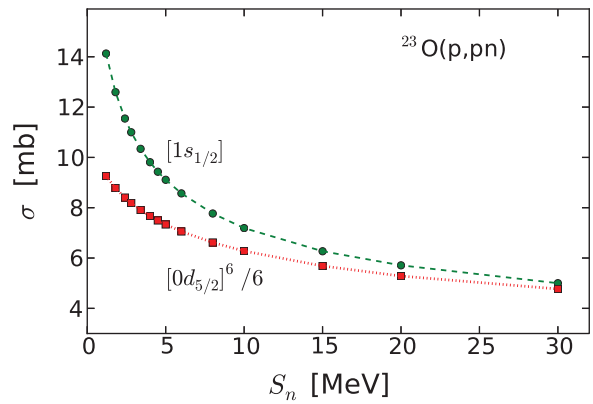

FIG. 7. (Color online) Cross sections for neutron removal in (p, pn) reactions on ^{23}O from $[0d_{5/2}]^6$ and $[1s_{1/2}]$ orbitals as a function of the separation energy. The cross sections for neutron removal from the $[0d_{5/2}]^6$ orbital is divided by the number of the neutrons in the orbital (6). The separation energies are varied artificially. The dashed and dotted curves are to guide the eyes.

knockout cross section. As the separation energy increases it becomes harder to knockout a neutron without rescattering effects.

We play a similar game as above in order to test the dependence of the cross sections on the matter distribution. To avoid inclusion of the dependence of the cross section on the separation energy, we assume a constant separation energy for the removed neutrons and protons. We also adopt the naive shell-model with eight protons in the $0f_{1/2}$ shell. The neutrons fill progressively the $0f_{5/2}$, $1p_{1/2}$, $0g_{9/2}$, and $0g_{7/2}$ orbitals. The neutron and proton densities for the Ni isotopes are calculated within the Hartree-Fock-Bogoliubov model using the SLy4 interaction [109] and a mixed pairing interaction (see Ref. [110]). Only even-even isotopes were considered. The neutron skin thickness is characterized by the difference of neutron and proton rms radii,

$$\delta r = \langle r_n^2 \rangle^{1/2} - \langle r_p^2 \rangle^{1/2}. \tag{38}$$

In Fig. 8 we show our results for the neutron skin of even-even Ni isotopes in the upper panel. The lower panel displays the (p, pn) and $(p, 2p)$ cross sections obtained assuming a fixed binding energy for the knocked out nucleon.

It is clear from Fig. 8 that the increasing neutron skin has a small effect on the $(p, 2p)$ cross sections, if the separation energy of the removed proton is kept constant. The main effect is to reduce the cross section due to the larger rescattering probability as the nuclear mass increases. The neutron-proton and proton-proton total cross sections are about the same at this energy. The large nuclear charge and the Coulomb barrier

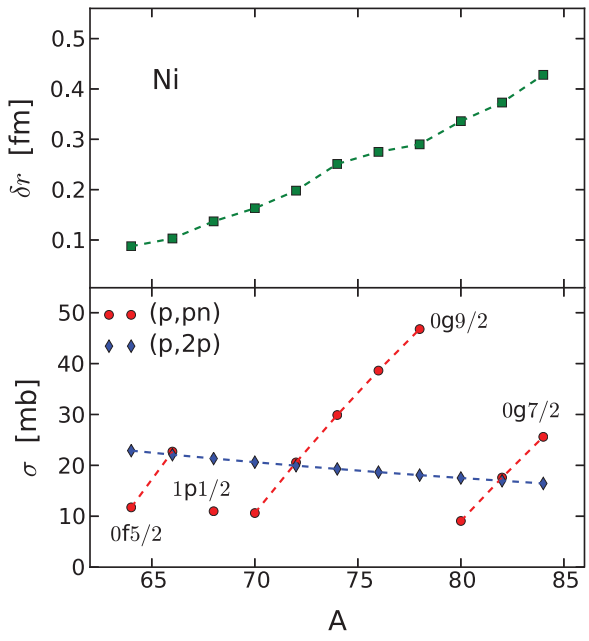

FIG. 8. (Color online) Neutron skin of even-even Ni isotopes obtained with a HFB calculation (upper panel). The lower panel displays the (p, pn) and $(p, 2p)$ cross sections on Ni isotopes at 500 MeV/nucleon assuming a fixed binding energy for the knocked out nucleon (see text for explanation). The dashed curves are to guide the eyes.

for the proton leads to a concentration of the proton wave function at the nuclear center where the absorption effects are stronger, yielding to a larger reduction of the $(p, 2p)$ cross section compared to (p, pn). However, the increasing neutron numbers in each orbital will increase the neutron removal probabilities as the orbital is filling up. This is clearly seen in the figure. In principle, the cross sections for neutron removal would increase even faster because an increasing neutron skin often means a smaller separation energy for a valence neutron. As we discussed in connection with Fig. 7, decreasing separation energies lead to increasing values of removal cross sections. Therefore, the dependence on the neutron skin should be manifest throughout the increasing number of neutrons in the orbitals and also with the separation energy of the removed neutron. For proton removal the increasing neutron skin has a lesser important role on the separation energy.

It is worthwhile to compare which parts of the wave function are accessible in knockout reactions with heavy ions with those obtained in (p, pN) reactions. The theory for knockout reactions with heavy ions, routinely used to extract nuclear spectroscopic information, relies on the eikonal theory developed in Ref. [37]. The theory is based on probability arguments using the eikonal S matrix to obtain the parts of the nucleon wave function which are "measured" by the reaction mechanism. It has later been proven to be a valuable tool for reactions involving unstable nuclear beams [38,40,48]. Following the same formalism as in Refs. [37,38,40] one obtains for the probability to remove a nucleon in orbital (jl) located at distance $\mathbf{b}$ (perpendicular to the collision axis) from the center of the projectile as

$$P_{jl}(b) = \frac{1}{2l+1} |S_c(b)|^2 \sum_m \int d^3\mathbf{r} |\psi_{jlm}(\mathbf{r})|^2 \times [1 - |S_n(\sqrt{r^2 \sin^2\theta + b^2 - 2rb \sin\theta \cos\phi})|^2]. \tag{39}$$

Here S_N (S_c) is the eikonal matrix amplitude for the scattering of the nucleon N (core c) on the target, and $\mathbf{r} \equiv (r, \theta, \phi)$.

In Fig. 9, upper panel, we show the dashed curve shows the probability for removal of a neutron in the reaction ^{12}C(^{68}Ni,^{67}Ni) at 500 MeV/nucleon as a function of the distance to the c.m. of ^{68}Ni. The dotted curve represents the removal probability in a ^{68}Ni(p, n) reaction at the same energy. For comparison the square of the radial wave function $u(r)$ is also shown (solid curve). We assume a neutron in the $0f_{7/2}$ orbital in ^{68}Ni, bound by 15.68 MeV. The figures in the middle panel are for the reactions ^{12}C(^{11}Be,^{10}Be) and ^{11}Be(p, n) at 500 MeV/nucleon. We assume a neutron in the $1s_{1/2}$ orbital in ^{11}Be, bound by 0.54 MeV. The figures in the lower panel are for the reactions ^{12}C(^{8}B,^{7}Be) and ^{8}Be$(p, 2p)$ at 500 MeV/nucleon. We assume a neutron in the $0p_{3/2}$ orbital in ^{8}Be, bound by 0.14 MeV. One observes that the removal cross sections for both knockout and (p, pn) reactions probe the surface part of the wave function. This is due to the fact that in both cases, the absorption is very strong for small impact parameters. For proton or neutron removal from even deeper bound states, with a concentration of the wave function closer

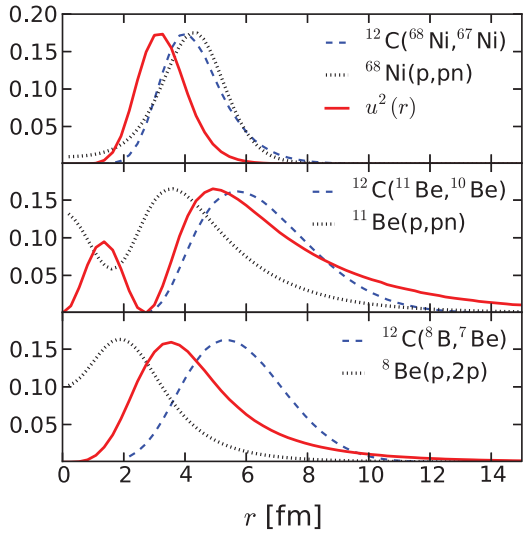

FIG. 9. (Color online) Upper panel: The dashed curve shows the probability for removal of a neutron in the reaction ^{12}C(^{68}Ni,^{67}Ni) at 500 MeV/nucleon as a function of the distance to the c.m. of ^{68}Ni. The dotted curve represents the removal probability in a ^{68}Ni(p, pn) reaction at the same energy. For comparison the square of the radial wave function $u(r)$ is also shown (solid curve). Middle panel: Same as the upper panel, but for the reactions ^{12}C(^{11}Be,^{10}Be) and ^{11}Be(p, pn) at 500 MeV/nucleon. Lower panel: Same as upper panel, but for the reactions ^{12}C(^{8}B,^{7}Be) and ^{8}B(p, $2p$) at 500 MeV/nucleon.

to the origin, both reaction mechanisms will probe an even smaller part of the wave function tail.

In the middle panel of Fig. 9 one sees that the part of the wave function probed in the ^{12}C(^{11}Be,^{10}Be) is again limited to the surface of the nucleus, beyond the orbital maximum density. On the other hand, the (p, pn) reaction has a much larger probability of accessing information on the inner part of the wave function, as seen by the dashed curve. These results are in agreement with the conclusions drawn in Ref. [28] for stable nuclei where it has been shown that for light nuclei the average density probed in (e, $e'p$) is comparable to the one probed in (p, $2p$). There is a strong A dependence, though, and for medium-heavy and heavy nuclei one is rather probing the surface region in (p, pN) reactions. It is thus clear that knockout reactions with heavy ions and (p, pN) reactions yield complementary nuclear spectroscopic information. For deep bound states the first reaction is only accessible to the tail of the nuclear wave function, whereas the (p, pN) reaction process probes the largest part of the wave function for loosely bound nuclei.

2. *Momentum distributions*

The shape of the momentum distributions for (p, $2p$) and (p, pn) reactions always have similar characteristics as those shown in Fig. 6, independent of the nucleus. As we have discussed before, for stable nuclei the shape will depend mainly on the angular momentum and on the separation energy of the knocked out nucleon. The dependence on the angular momentum is obvious, following the same trend for either stable or unstable projectiles. But unstable projectiles often

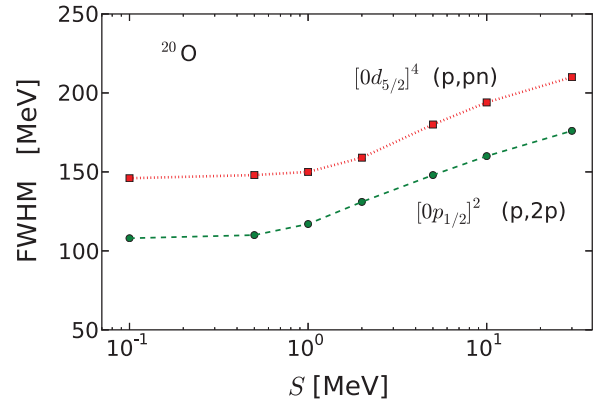

FIG. 10. (Color online) Full width at half-maximum (FWHM) of the transverse momentum distributions in (p, $2p$) and (p, pn) reactions of ^{20}O at 500 MeV/nucleon as a function of the proton and neutron separation energies. The upper curve is for (p, pn) and lower curve for (p, $2p$) reactions. The separation energies are varied artificially (see text for explanation). The dashed and dotted curves are to guide the eyes.

exhibit very low nucleon separation energies. As with nucleon removal reactions with heavy ions, one also expects that the width of the momentum distribution are strongly dependent on the separation energy, in particular close to the drip line. We will test this with ^{20}O which has a proton (neutron) separation energy of 19.43 (7.61) MeV. We will artificially vary these values to learn how the widths of the transverse momentum distributions will vary with the separation energy. The knocked out protons and neutrons are assumed to occupy the $[0p_{1/2}]^2$ and $[0d_{5/2}]^4$ levels, respectively.

In Fig. 10 we show the full width at half-maximum (FWHM) of the transverse momentum distributions in (p, $2p$) and (p, pn) reactions of ^{20}O at 500 MeV/nucleon as a function of the proton and neutron separation energies. The upper curve is for (p, pn) and lower curve for (p, $2p$) reactions. As expected, the widths for d states are larger than those for p states.

A very different trend exists for (p, pN) reactions in comparison to nucleon knockout reactions induced by heavy ions. For the latter case, the width of the momentum distributions decreases strongly with decreasing separation energies. That was in fact, one of the hallmarks for the identification of the first halo nuclei [36]. In contrast, one observes in Fig. 10 a "saturation" of the width for decreasing separation energy. The reason for this behavior is the fact that knockout reactions induced by heavy ions are a very peripheral process, being almost entirely sensitive to the tail of the nucleon wave functions [38]. In contrast, (p, pN) reactions are in great part influenced by the part of the nucleon wave function inside the nucleus. The width of the momentum distributions for (p, pN) reactions reduce with decreasing separation energies because an extended part of the nucleon wave function is accessed as the separation energy decreases till a "saturation" of the width is reached at low separation energies. As concluded from our calculations (see, e.g., Fig. 7), the total cross section is a better measure of the nucleon separation energy in loosely bound nuclei.

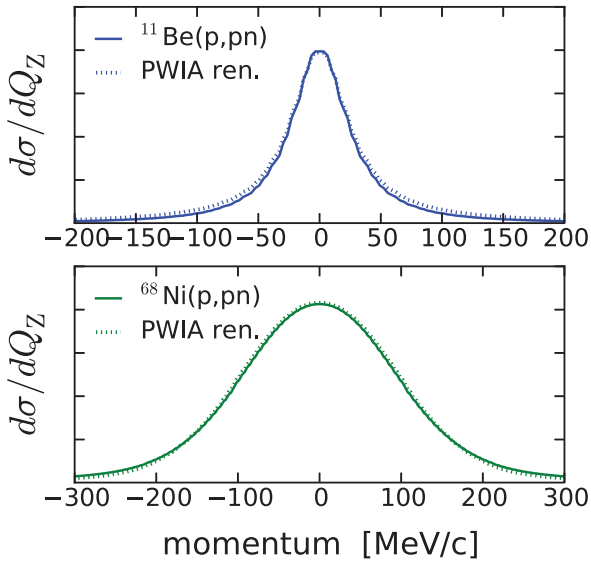

FIG. 11. (Color online) Longitudinal momentum distributions for ^{11}Be(p,n) and ^{68}Ni(p,n) reactions at 500 MeV/nucleon. For ^{11}Be we assume neutron removal from the $1s_{1/2}$ states with 0.502 MeV separation energy, while for ^{68}Ni we assume the removal from $0f_{3/2}$ orbital with separation energy of 15.68 MeV. PWIA results are shown as dashed lines, whereas the solid lines are for the full DWIA.

Finally, in Figs. 11 and 12 we show the longitudinal (Fig. 11) and transverse (Fig. 12) momentum distributions for ^{11}Be(p,n) and ^{68}Ni(p,n) reactions at 500 MeV/nucleon. For ^{11}Be we assume neutron removal from the $1s_{1/2}$ state with 0.502 MeV separation energy, while for ^{68}Ni we assume the removal from $0f_{7/2}$ orbital with separation energy of 15.68 MeV. In the plane wave impulse approximation (PWIA), the S matrices for the incoming and outgoing particles are all

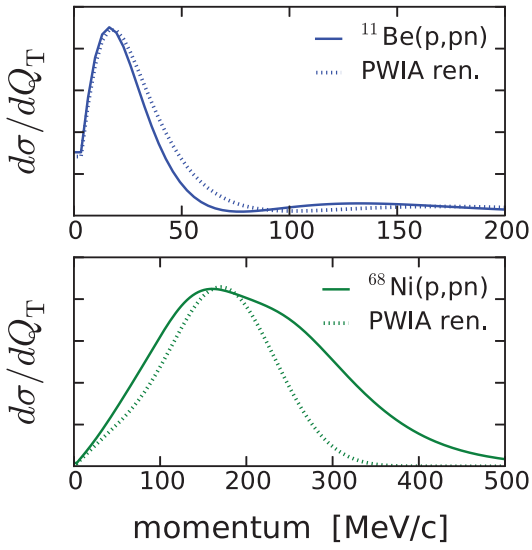

FIG. 12. (Color online) Same as in Fig. 11, but for transverse momentum distributions.

set to the unity (no distortion). From Eq. (25) we get

$$\left(\frac{d\sigma}{d^3Q}\right)_{\rm PWIA} = \frac{1}{(2\pi)^3}\frac{S(lj)}{2j+1}\sum_m \left\langle \frac{d\sigma_{pN}}{d\Omega}\right\rangle_Q \times \left|\int d^3\mathbf{r}\, e^{-i\mathbf{Q}\mathbf{r}}\psi_{jlm}(\mathbf{r})\right|^2. \quad (40)$$

In Figs. 11 and 12 the PWIA results are shown as dashed lines, whereas the solid lines are for the full DWIA, Eq. (25). As we have discussed in connection with Fig. 5, the PWIA yields results that are much larger than in the DWIA, because the absorption is missing in the PWIA method. Hence, we renormalize the results to be shown in the same plot. It is clear from Fig. 11 that the shape of the longitudinal momentum distributions is insensitive to the details of the wave function being probed. The two cases compared (^{11}Be and ^{68}Ni) are very representative because they differ strongly on the separation energies, angular momenta, and on principal quantum numbers (number of nodes in the wave functions). In both cases, the insensitivity of the width is manifest. The physical reason is the same as for longitudinal momentum distributions in knockout reactions, first shown in Ref. [38]. This is easily understood from Eq. (31) because the dependence on Q_z is basically contained in the last integral: the S matrices and in medium quasifree cross sections are weakly dependent on Q_z. Their net effect is to rescale the magnitude of the total cross section.

For the transverse momentum distributions, we see a clear separation of shapes in Fig. 12, as they are appreciably influenced by the S matrices which enter directly into the b integral in Eq. (33). Some of the features of the wave distortion in the entrance and outgoing channels carry a stamp on the transverse momentum distributions, as seen in the upper panel of the figure where a shoulder in the tail of the distributions is clearly seen. This is the same sort of reaction distortion mechanism occurring in heavy ion knockout reactions which was emphasized in Ref. [45]. The contribution of the different m magnetic substates also impact on the shape of the distributions. The DWIA and PWIA results look different, mostly visible as a shift of the curve for ^{11}Be$(p,\ pn)$, or strongly distorted, as in the case of ^{68}Ni$(p,\ pn)$ seen in the lower panel of Fig. 12.

V. CONCLUSIONS

There are other observables which have been used for nuclear spectroscopy with $(p,\ pN)$ reactions. In the past, angular distribution of the nucleons have been scrutinized by comparison with theory. The comparison in this case is more sensitive to several details of the theory model. It has been indeed a difficult task to learn from experiments which physical input was determinant for a good reproduction of the angular data [1]. We believe that a much simpler method can be used based on momentum distributions, which also have been shown to be very useful in the case of heavy ion reactions.

One also probes the spectroscopy of nuclei more closely if one measure both $(p, 2p)$ and (p, pn) reactions and studies cross section ratios such as

$$\mathcal{R} = \frac{(d\sigma/dQ)_{(p,pn)}\left(d\sigma_{pp}^{\rm elast}/d\Omega\right)_{\theta=90^\circ}}{(d\sigma/dQ)_{(p,pn)}\left(d\sigma_{pn}^{\rm elast}/d\Omega\right)_{\theta=90^\circ}}. \quad (41)$$

In fact, similar methods have been introduced in the past to separate the effects of final state interactions and off-shell effects in $(p, 2p)$ and (p, pn) cross sections at $E_p < 100$ MeV [111–114].

In this paper we have focused on the opportunities that $(p, 2p)$ and (p, pn) reactions can offer to the studies of nuclei far from the stability line in experiments using inverse kinematics. Quasifree $(p, 2p)$ and (p, pn) reactions have been used as a spectroscopic tool for more than 60 years. The reaction mechanism is known to be well described in the distorted wave impulse approximation formalism. We have developed a formalism making use of the eikonal theory allowing a quantitative description of the reaction mechanism including absorption from the elastic channel due to multiple-scattering effects. Our approach provides scattering-angle averaged cross sections and recoil momentum distributions, well adapted to the needs of large-acceptance experiments in inverse kinematics with radioactive beams.

Here we concentrated on the use of momentum distributions as a spectroscopic tool, following the success of using nucleon knockout reactions for nuclear spectroscopy of radioactive beams. In fact, we have shown that (p, pN) reactions show some similarities with heavy-ion knockout reactions. But some striking differences are also found. Perhaps the most evident one is that fact that (p, pN) reactions are more sensitive to the interior part of the nuclear wave function. This carries imprints in the momentum distributions that are easily understood by using an eikonal and DWIA reaction formalism. In view of the development and better experimental detection techniques, data are now of much higher quality than those obtained in previous decades. Pioneering experiments with (p, pN) with radioactive nuclei in inverse kinematics are now becoming available. In this article we have shown the main reaction mechanism features which are expected, and what can be learned from the properties of single particle states. More exclusive measurements will require more detailed reaction theory, which is now under development.

ACKNOWLEDGMENTS

We acknowledge beneficial discussions with Valerii Panin and Stephanos Paschalis. This work was partially supported by the US DOE Grants No. DE-FG02-08ER41533 and No. DE-FG02-10ER41706. One of the authors (C.B.) acknowledges the Helmholtz International Center for FAIR (HIC for FAIR) and the ExtreMe Matter Institute EMMI for supporting his visits to the Technische Universität Darmstadt, where much of this work was done.

[1] G. Jacob and Th. A. J. Maris, Rev. Mod. Phys. **38**, 121 (1966); **45**, 6 (1973).
[2] P. Kitching, W. J. McDonald, Th. A. J. Maris, and C. A. Z. Vasconcellos, Adv. Phys. Part. Nuclei **15**, 43 (1985).
[3] P. G. Hansen and J. A. Tostevin, Annu. Rev. Nucl. Part. Sci. **53**, 219 (2003).
[4] A. Gade *et al.*, Phys. Rev. C **77**, 044306 (2008).
[5] C. Barbieri and W. H. Dickhoff, Int. J. Mod. Phys. A **24**, 2060 (2009); arXiv:0901.1920[nucl-th].
[6] O. Jensen, G. Hagen, M. Hjorth-Jensen, B. A. Brown, and A. Gade, Phys. Rev. Lett. **107**, 032501 (2011).
[7] T. Frick, H. Muther, A. Rios, A. Polls, and A. Ramos, Phys. Rev. C **71**, 014313 (2005).
[8] Letter of Intent of the R3B Collaboration, http://www-land.gsi.de/r3b/.
[9] T. Aumann, Prog. Part. Nucl. Phys. **59**, 3 (2007).
[10] T. Kobayashi *et al.*, Nucl. Phys. **805**, 431c (2008).
[11] V. Panin *et al.*, GSI Sci. Rep. **2012**, PHN-ENNA-EXP-27 (2013).
[12] N. S. Chant and P. G. Roos, Phys. Rev. C **15**, 57 (1977).
[13] N. S. Chant and P. G. Roos, Phys. Rev. C **27**, 1060 (1983).
[14] A. K. Kerman, H. McManus, and R. M. Thaler, Ann. Phys. (NY) **8**, 551 (1959).
[15] G. Bertsch, J. Borysowicz, H. McManus, and W. G. Love, Nucl. Phys. A **284**, 399 (1977).
[16] J. P. Jeukenne, A. Lejeune, and C. Mahaux, Phys. Rev. C **16**, 80 (1977).
[17] W. G. Love and M. A. Franey, Phys. Rev. C **24**, 1073 (1981).
[18] N. Yamaguchi, S. Nagata, and J. Michyama, Prog. Theor. Phys. **70**, 459 (1983).
[19] T. Cheon, K. Takayanagi, and K. Yakaki, Nucl. Phys. A **445**, 227 (1985).
[20] M. A. Franey and W. G. Love, Phys. Rev. C **31**, 488 (1985).
[21] C. J. Horowitz and M. J. Iqbal, Phys. Rev. C **33**, 2059 (1986).
[22] K. Nakayama and W. G. Love, Phys. Rev. C **38**, 51 (1988).
[23] G. Jacob, Th. A. J. Maris, C. Schneider, and M. R. Teodoro, Nucl. Phys. A **257**, 517 (1976).
[24] G. Krein, Th. A. J. Maris, B. B. Rodrigues, and E. A. Veit, Phys. Rev. C **51**, 2646 (1995).
[25] B. Van Overmeire, W. Cosyn, P. Lava, and J. Ryckebusch, Phys. Rev. C **73**, 064603 (2006).
[26] Bart Van Overmeire, Ph.D. thesis, Ghent University, 2007.
[27] Wim Cosyn and Jan Ryckebusch, Phys. Rev. C **80**, 011602(R) (2009).
[28] J. Ryckebusch, W. Cosyn, and M. Vanhalst, Phys. Rev. C **83**, 054601 (2011).
[29] M. Vanhalst, J. Ryckebusch, and W. Cosyn, Phys. Rev. C **86**, 044619 (2012).
[30] D. F. Jackson, Phys. Scr. **25**, 514 (1982).
[31] B. K. Jain, J. Phys. G **5**, 663 (1979).
[32] C. Samanta, N. S. Chant, P. G. Roos, A. Nadasen, J. Wesick, and A. A. Cowley, Phys. Rev. C **34**, 1610 (1986).
[33] D. F. Jackson, Nucl. Phys. A **257**, 221 (1976).
[34] Th. A. J. Maris, Nucl. Phys. **9**, 577 (1958).
[35] M. S. Hussein, R. A. Rego, and C. A. Bertulani, Phys. Rep. **201**, 279 (1991).
[36] I. Tanihata *et al.*, Phys. Rev. Lett. **55**, 2676 (1985).
[37] M. Hussein and K. McVoy, Nucl. Phys. A **445**, 124 (1985).
[38] C. A. Bertulani and K. W. McVoy, Phys. Rev. C **46**, 2638 (1992).

[39] N. A. Orr *et al.*, Phys. Rev. Lett. **69**, 2050 (1992).
[40] K. Hencken, G. Bertsch, and H. Esbensen, Phys. Rev. C **54**, 3043 (1996).
[41] T. Aumann *et al.*, Phys. Rev. Lett. **84**, 35 (2000).
[42] Y. L. Parfenova, M. V. Zhukov, and J. S. Vaagen, Phys. Rev. C **62**, 044602 (2000).
[43] A. Ozawa, T. Suzuki, and I. Tanihata, Nucl. Phys. A **693**, 32 (2001).
[44] D. Cortina-Gil *et al.*, Phys. Rev. Lett. **93**, 062501 (2004).
[45] C. A. Bertulani and P. G. Hansen, Phys. Rev. C **70**, 034609 (2004).
[46] C. A. Bertulani and A. Gade, Comput. Phys. Commun. **17**, 372 (2006).
[47] R. Kanungo *et al.*, Phys. Rev. Lett. **102**, 152501 (2009).
[48] Alexandra Gade and Jeffrey A. Tostevin, Nucl. Phys. News, **20**, 11 (2010).
[49] C. Rodriguez-Tajes *et al.*, Phys. Rev. C **83**, 064313 (2011).
[50] G. Baur, Phys. Lett. B **178**, 135 (1986).
[51] C. Spitaleri *et al.*, Phys. Rev. C **63**, 055801 (2001).
[52] C. Spitaleri *et al.*, Nucl. Phys. A **719**, 99c (2003).
[53] S. Typel and G. Baur, Ann. Phys. (NY) **305**, 228 (2003).
[54] C. Spitaleri *et al.*, Phys. Rev. C **69**, 055806 (2004).
[55] M. La Cognata *et al.*, Phys. Rev. C **76**, 065804 (2007).
[56] R. Pizzone *et al.*, Phys. Rev. C **87**, 025805 (2013).
[57] I. E. McCarthy and K. L. Lim, Phys. Rev. **133**, B1006 (1964).
[58] I. E. McCarthy and K. L. Lim, Nucl. Phys. **88**, 433 (1966).
[59] C. A. Bertulani, Hongliang Liu, and H. Sagawa, Phys. Rev. C **85**, 014321 (2012).
[60] C. A. Bertulani, H. F. Lu, and H. Sagawa, Phys. Rev. C **80**, 027303 (2009).
[61] W.-M. Yao *et al.*, J. Phys. G **33**, 1 (2006).
[62] C. A. Bertulani and C. De Conti, Phys. Rev. C **81**, 064603 (2010).
[63] E. Clementel and C. Villi, Il Nuovo Cimento **1**, 176 (1955).
[64] C. A. Bertulani, Braz. J. Phys. **16**, 380 (1986).
[65] G. Q. Li and R. Machleidt, Phys. Rev. C **48**, 1702 (1993).
[66] G. Q. Li and R. Machleidt, Phys. Rev. C **49**, 566 (1994).
[67] Cai Xiangzhou, Feng Jun, Shen Wenqing, Ma Yugang, Wang Jiansong, and Ye Wei, Phys. Rev. C **58**, 572 (1998).
[68] C. A. Bertulani, J. Phys. G **27**, L67 (2001).
[69] B. Chen, F. Sammarruca, and C. A. Bertulani, Phys. Rev. C **87**, 054616 (2013).
[70] E. F. Redish, G. J. Stephenson, Jr., and G. M. Lerner, Phys. Rev. **2**, 1665 (1970).
[71] P. G. Roos, N. S. Chant, A. A. Cowley, D. A. Goldberg, H. D. Holmgren, and R. Woody, Phys. Rev. C **15**, 69 (1977).
[72] V. S. Barashenkov and V. M. Maltsev, Fortschr. Phys. **9**, 549 (1961).
[73] V. G. J. Stoks, R. A. M. Klomp, M. C. M. Rentmeester, and J. J. de Swart, Phys. Rev. C **48**, 792 (1993).
[74] R. A. Arndt, I. I. Strakovsky, and R. L. Workman, Int. J. Mod. Phys. A **18**, 449 (2003).
[75] Center for Nuclear Studies, Data Analysis Center, http://gwdac.phys.gwu.edu/.
[76] D. L. Olson, B. L. Berman, D. E. Greiner, H. H. Heckman, P. J. Lindstrom, and H. J. Crawford, Phys. Rev. C **28**, 1602 (1983).
[77] W. R. Webber *et al.*, Astrophys. J. **508**, 940 (1998).
[78] W. R. Webber and J. C. Kish, in *Proceedings of the 19th International Cosmic Ray Conference, La Jolla, CA, 1985* (NASA, 1985), Vol. 5.
[79] W. R. Webber, J. C. Kish, and D. A. Schrier, Phys. Rev. C **41**, 520 (1990); **41**, 547 (1990).
[80] W. E. Crandall *et al.*, Phys. Rev. **101**, 329 (1956).
[81] V. Parikh *et al.*, Nucl. Phys. **18**, 628 (1960).
[82] W. E. Burcham *et al.*, Proc. Phys. Soc. London, Sect. A **68**, 1001 (1955).
[83] A. H. Rosenfeld *et al.*, Phys. Rev. **103**, 413 (1956).
[84] K. Goebel *et al.*, Nucl. Phys. **24**, 28 (1961).
[85] J. B. Cumming *et al.*, Phys. Rev. **111**, 1386 (1958).
[86] N. Horwitz and J. J. Murray, Phys. Rev. **117**, 1361 (1960).
[87] P. A. Benioff, Phys. Rev. **119**, 316 (1960).
[88] A. Korejwo, M. Giller, T. Dzikowski, V. V. Perelygin, and A. V. Zarubin, J. Phys. G **28**, 1199 (2002).
[89] S. Das *et al.*, Nucl. Phys. A **190**, 501 (1972).
[90] Particle Data Group, http://pdg.lbl.gov/.
[91] M. L. Webb *et al.*, Phys. Rev. C **36**, 193 (1987).
[92] R. Silberberg, C. H. Tsao, and A. F. Barghouty, Astrophys. J. **501**, 911 (1998).
[93] Th. A. J. Maris, M. R. Teodoro, and C. A. Z. Vasconcellos, Nucl. Phys. A **322**, 461 (1979).
[94] Y. Kudo and K. Miyazaki, Phys. Rev. C **34**, 1192 (1986).
[95] A.W. Stetz, Phys. Rev. C **21**, 1979 (1980).
[96] L. Chulkov *et al.*, Nucl. Phys. A **759**, 43 (2005).
[97] A. A. Cowley *et al.*, Phys. Rev. Lett. **45**, 1930 (1980).
[98] G. Ciangaru *et al.*, Phys. Rev. C **27**, 1360 (1983).
[99] A. A. Cowley *et al.*, Phys. Lett. B **201**, 196 (1988).
[100] J. V. Pilcher, A. A. Cowley, D. M. Whittal, and J. J. Lawrie, Phys. Rev. C **40**, 1937 (1989).
[101] A. A. Cowley *et al.*, Europhys. Lett. **13**, 37 (1990).
[102] S. V. Fortsch, A. A. Cowley, J. J. Lawrie, J. V. Pilcher, F. D. Smit, and D. M. Whittal, Phys. Rev. C **48**, 743 (1993).
[103] G. Ciangaru, Phys. Rev. C **30**, 479 (1984).
[104] A. A. Cowley *et al.*, Phys. Rev. C **57**, 3185 (1998).
[105] G. F. Steyn, Acta Phys. Pol. **30**, 527 (1999).
[106] H. Feshbach, A. Kerman, and S. Koonin, Ann. Phys. (NY) **125**, 429 (1980).
[107] I. Tanihata, S. Nagamia, S. Schnetzer, and H. Steiner, Phys. Lett. B **100**, 121 (1981).
[108] J. Mougey *et al.*, Nucl. Phys. A **262**, 461 (1976).
[109] E. Chabanat, P. Bonche, P. Haensel, J. Meyer, and R. Schaeffer, Nucl. Phys. A **635**, 231 (1998).
[110] G. F. Bertsch, C. A. Bertulani, W. Nazarewicz, N. Schunck, and M. V. Stoitsov, Phys. Rev. C **79**, 0343306 (2009).
[111] N. I. Woloshin *et al.*, Izv. Acad. Nauk CCCP, ser. z. **57**, 218 (1993).
[112] V. B. Shostak *et al.*, Nucl. Phys. A **643**, 3 (1998).
[113] V. B. Shostak *et al.*, Phys. Rev. C **61**, 024601 (1999).
[114] V. B. Shostak *et al.*, Braz. J. Phys. **31**, 327 (2001).